Correlation of Tumor Hypoxia Metrics Derived from ^{18}F-Fluoromisonidazole Positron Emission Tomography and Pimonidazole Fluorescence Images of Optically Cleared Brain Tissue

Matthew L. Scarpelli[1], Debbie R. Healey[1], Alberto Fuentes[1], Vikram D. Kodibagkar[2], and C. Chad Quarles[1]

[1]Barrow Neuroimaging Innovation Center, Barrow Neurological Institute, St. Joseph's Hospital and Medical Center, Phoenix, AZ; and [2]School of Biological and Health Systems Engineering, Arizona State University, Tempe, AZ

Corresponding Author:
Matthew L. Scarpelli, PhD
Barrow Neuroimaging Innovation Center, Barrow Neurological Institute, St. Joseph's Hospital and Medical Center, 350 W. Thomas Rd, Phoenix, AZ 85013;
E-mail: matthew.scarpelli@barrowneuro.org

Key Words: Tumor, hypoxia, FMISO, PET, tissue clearing

Abbreviations: ^{18}F-fluoromisonidazole (FMISO), positron emission tomography (PET), magnetic resonance imaging (MRI), T2-weighted (T2W), intraperitoneal (IP), intravenous (IV), phosphate buffer (PB), maximum tumor-to-cerebellar ratio (TCmax), maximum standardized uptake value (SUVmax)

ABSTRACT

^{18}F-fluoromisonidazole (FMISO) positron emission tomography (PET) is a widely used noninvasive imaging modality for assessing hypoxia. We describe the first spatial comparison of FMISO PET with an ex vivo reference standard for hypoxia across whole tumor volumes. Eighteen rats were orthotopically implanted with C6 or 9L brain tumors and made to undergo FMISO PET scanning. Whole brains were excised, sliced into 1-mm-thick sections, optically cleared, and fluorescently imaged for pimonidazole using an in vivo imaging system. FMISO maximum tumor uptake, maximum tumor-to-cerebellar uptake (TCmax), and hypoxic fraction (extracted 110 minutes after FMISO injection) were correlated with analogous metrics derived from pimonidazole fluorescence images. FMISO SUVmax was not significantly different between C6 and 9L brain tumors ($P = .70$), whereas FMISO TCmax and hypoxic fraction were significantly greater for C6 tumors ($P < .01$). FMISO TCmax was significantly correlated with the maximum tumor pimonidazole intensity ($\rho = 0.76$, $P < .01$), whereas FMISO SUVmax was not. FMISO tumor hypoxic fraction was significantly correlated with the pimonidazole-derived hypoxic fraction ($\rho = 0.78$, $P < .01$). Given that FMISO TCmax and tumor hypoxic fraction had strong correlations with the pimonidazole reference standard, these metrics may offer more reliable measures of tumor hypoxia than conventional PET uptake metrics (SUVmax). The voxel-wise correlation between FMISO uptake and pimonidazole intensity for a given tumor was strongly dependent on the tumor's TCmax ($\rho = 0.81$, $P < .01$) and hypoxic fraction ($\rho = 0.85$, $P < .01$), indicating PET measurements within individual voxels showed greater correlation with pimonidazole reference standard in tumors with greater hypoxia.

INTRODUCTION

Tumor hypoxia is associated with worse clinical outcomes and has been implicated in tumor resistance to radiotherapy and chemotherapy (1–5). In the hopes of improving prognostication and therapeutic planning, a variety of techniques for measuring tumor hypoxia have been proposed and or evaluated. For example, a variety of noninvasive techniques for measuring hypoxia have been developed using positron emission tomography (PET) or magnetic resonance imaging (MRI) (6–10). These imaging techniques might be used, for example, to modify therapy based on the hypoxic status of a tumor (11, 12). ^{18}F-fluoromisonidazole (FMISO) PET is one of the most widely studied imaging methods for measuring chronic hypoxia in tumors (5, 6, 13–20). FMISO freely diffuses into cells where its nitro functional group has an affinity for electrons produced in the electron transport chain. In cells with low oxygen levels, these electrons react with the FMISO nitro functional group to form an alkylating agent that binds to intracellular macromolecules, effectively trapping the radiotracer within hypoxic cells (21). Studies in cell cultures have shown that FMISO uptake increases up to 15-fold when going from normoxic to hypoxic conditions (3.5 mm Hg O_2) (22). Although these imaging techniques hold great potential, these have uncertainties (eg, limited spatial

ISSN 2379-1381 https://doi.org/10.18383/j.tom.2020.00046

resolution, variations in contrast agent delivery/retention) that diminish the reliability of image-derived hypoxia measurements (23–25).

Histologic analyses of resected tissue provide ex vivo measurements that are well-established measurements of tumor hypoxia. This includes optical imaging of externally administered nitroimidazole agents that are trapped intracellularly in areas of hypoxia (26). One of the most widely used agents is pimonidazole, which, after injection, forms adducts within hypoxic cells. Antibodies for pimonidazole have been developed that enable immunohistochemical or immunofluorescent detection of the pimonidazole adducts in resected tissue (21). Pimonidazole is believed to be sensitive to hypoxic cells with oxygen tension <10 mm Hg O_2 (27–29). The high specificity and sensitivity of these immunohistologic or immunofluorescent measurements make them useful for validating hypoxia measurements derived from in vivo imaging modalities such as PET or MRI (8, 18, 19, 30, 31). However, owing to differences in scale, it is difficult to directly compare in vivo medical images (slice thickness on the order of millimeters) and ex vivo histologic measurements (slice thickness on the order of micrometers). Consequently, few studies have cross-validated in vivo PET or MRI hypoxia metrics with ex vivo reference standards for hypoxia across whole tumor volumes.

This study aims to address this knowledge gap by using a recently developed methodology that coregisters in vivo medical images with ex vivo fluorescent images of optically cleared tissue (32). Optical tissue clearing overcomes the light penetration issues that prevent optical imaging of thick tissue sections, facilitating the assessment of tumor hypoxia in larger sections of resected tissue. Here, this method is used to cross-validate in vivo measures of hypoxia (FMISO PET) with ex vivo measures of hypoxia (pimonidazole immunofluorescence) across whole tumor volumes. Preclinical brain tumor models that have high (C6 glioma) and low (9L gliosarcoma) levels of hypoxia are used (7, 33–35). The in vivo and ex vivo hypoxia measurements are compared across whole tumor volumes, providing insight into their regional agreement and potential for clinical application.

METHODS

Animals and Disease Models

C6 and 9L cells were harvested and resuspended in phosphate buffer (PB) saline at a concentration of ~15 million cells/mL. A total of 4 uL of cell suspension was then orthotopically implanted in 5- to –9-week-old Wistar (C6) and Fisher (9L) rats purchased from Charles River Laboratories (Wilmington, MA). In total, 18 rats were implanted with tumors ($n = 8$ for 9L and $n = 10$ for C6) and made to undergo FMISO PET and T2-weighted (T2W) MRI scanning. The St. Joseph Hospital and Medical Center's Institutional Animal Care and Use Committee approved of all experimental procedures performed in this study, and all animals were treated humanely in accordance with the Laboratory Animal Welfare Act.

In Vivo PET and MRI

In vivo imaging was performed 25–46 days after implantation of 9L tumor cells and 18–21 days after implantation of C6 tumor cells. PET was performed using a Bruker Albira Si 3 ring preclinical PET scanner. A total of ~13 MBq of FMISO was injected either intraperitoneally ($n = 8$ total; 4 with C6 tumor and 4 with 9L tumors) or intravenously ($n = 10$ total; 6 with C6 tumor and 4 with 9L tumors). The intraperitoneal (IP) injections were performed owing to low concentrations of PET tracer that arose after scanning multiple subjects in a single day. The low concentrations of PET tracer required larger injection volumes that surpassed the institutional limits for intravenous (IV) injections, and consequently required IP injections.

Dynamic PET scans were acquired from 0 to 115 minutes after IV injection of tracer or from 5 to 120 minutes for IP injections. For all PET scans, the brain was positioned at the center of the field of view. An ordered subset expectation maximization algorithm was used for PET image reconstruction. Reconstructed PET images included corrections for scatter, dead time, and decay of tracer.

MRI was performed with a 7 T Bruker Biospec preclinical MRI scanner (Bruker Corporation, Billerica, MA). MRI scanning was performed immediately following completion of the PET scan. Animals were kept sedated when transferred between PET and MRI scanners and were made to remain in position on the same Bruker multimodality rat bed. To enable accurate coregistration between the MRI and PET images, we placed a fiducial phantom filled with water and PET tracer beneath the rat in the multimodality bed to act as a landmark (32). During MRI and PET, the rats were kept sedated, with airflow of 1–1.5 mL/s with 1%–3% isoflurane. MRI lasted ~15 minutes and included T2W rapid acquisition with relaxation enhancement, with a repetition time of 6500 milliseconds, echo time of 50 milliseconds, and a voxel size of $0.25 \times 0.25 \times 0.5$ mm^3.

Tissue Preparation

Following in vivo PET and MRI, 13 of the 18 rats were sacrificed via transcardiac perfusion with 150 mL of 100 U/mL heparinized PB to clear the blood from the system. This procedure was followed by 4% paraformaldehyde to fix the tissue (300 mL). One hour before perfusion, the rats were injected intraperitoneally with pimonidazole at 60 mg/kg, for ex vivo assessment of hypoxia. Once perfusion was complete, the brain was dissected and immersed in 4% paraformaldehyde for an additional 24–36 hours to complete the fixation process. After immersion in paraformaldehyde, the tissue was washed with 0.1-M PB and stored in 0.1-M PB.

Ex Vivo MRI and Tissue Slicing

Ex vivo MRI was performed on the excised rodent brains to enable registration of in vivo and ex vivo images. During the MRI scan, whole brains were secured within a pathology slice block (Acrylic Brain Slicer Matrix, Zivic Instruments, Pittsburgh, PA) and placed within a cylindrical tube filled with PB. MRI acquisition was set so that the MRI slices were aligned parallel to the slices of the pathology slice block. Ex vivo MRI included the same parameters as the in vivo MRI. Immediately following the MRI, the slice block with the brain was removed from the cylindrical tube, and the brain was sliced into 1-mm coronal slices. Each brain slice was then placed in 0.1-M PB in preparation for optical clearing. The brains were sliced into 1-mm slices because it was

the thinnest size available in the acrylic MRI-compatible slice block.

Optical Clearing and Pimonidazole

A clear, unobstructed brain imaging cocktail–based protocol was used in clearing the tissue slices as described previously (32). Following clearing tissue, slices were then washed in 0.1-M PB and incubated at 4°C for 3 days in 0.1-M PB with 0.1% triton-X and a 1:50 dilution of mouse IgG1 antipimonidazole (anti-Pimo) monoclonal antibody conjugated with fluorescein isothycyanate (FITC) (HP FITC Mab-1, Hypoxyprobe, Burlington, MA). After the 3-day incubation, the unbound antibody was washed from the tissue slices with 0.1-M PB at room temperature.

Ex Vivo Fluorescence Imaging

Optically cleared brain slices were imaged using an in vivo imaging system Spectrum (PerkinElmer, Waltham, MA). For in vivo imaging system, each set of brain slices were placed in a 12-well tissue culture plate filled with EasyIndex for refractive index matching (LifeCanvas Technologies, Cambridge, MA). An excitation wavelength of 500 nm and an emission wavelength of 540 nm were used for imaging anti-Pimo FITC. All in vivo imaging system imaging consisted of a 60-second acquisition with a bin size of 1 (corresponding to 34.4-μm pixels), F/Stop of 8, and field of view of 6.6 × 6.6 cm. In total, 2 acquisitions per brain were required to ensure the field of view covered the entire 12-well plate. The resulting fluorescence images have units of radiant efficiency (ie, photons/s/unit area/unit steradian/wattage of excitation laser).

Image Registration

All registrations were performed in 3D Slicer v4.10.1 (Cambridge, MA) using our previously developed multimodality registration methodology that is briefly described here (32). In vivo PET and MRI images were rigidly registered using the fiducial phantom placed within the Bruker multimodality rat bed. In vivo MRI images were then registered to ex vivo MRI images using an affine registration (with 12° of freedom). The resulting transformation was also applied to register the PET to the ex vivo MRI. The fluorescence images of optically cleared brain slices were registered slice by slice to the ex vivo MRI slices using the pathology slice block as a reference. This involved a landmark-based registration where 6 points were manually placed along the edges of the brain in each image. A 3D slicer's landmark registration module was used to calculate the geometric transform that most closely aligned the corresponding landmarks placed within the 2 images. After registration, all images were in the frame of reference of the ex vivo MRI with matching 1-mm-thick slices. The accuracy of this multimodality registration was assessed previously, where it was found to produce registered images with corresponding image features being at a median distance of 400 µm apart (32).

Image and Statistical Analysis

Tumor regions of interest were manually segmented using the hyperintense regions on the T2W MRI as a guide. Spherical volumes of interest (~45 mm^3) were placed within the cerebellum. PET image voxels were corrected for injected dose and rat weight to give standardized uptake values (SUVs). The median tumor and cerebellar SUVs were extracted for each rat (SUVmedian) and summarized across all subjects by taking the median SUVmedian (Figure 1). Owing to the tendency for distributions of tumor SUVs to deviate significantly from normality, nonparametric statistics were used in most of the analyses (including use of median values and nonparametric statistical tests) (36, 37). However, to enable comparison with previous literature, the mean tumor and cerebellar SUVs were also extracted (SUVmean) and summarized for all subjects by taking the mean SUVmean (see online supplemental Figure 1).

Before image registration, the maximum tumor uptake was extracted for each rat (SUVmax). The SUVmax was divided by the mean cerebellar uptake to give tumor-to-cerebellar ratios (TCmax), as this has been proposed as a measure of hypoxia (6, 14). The SUVmax and TCmax were extracted from 10-minute PET frames acquired at 60 and 110 minutes after FMISO injection (which differs from the 20-minute frame duration used in the

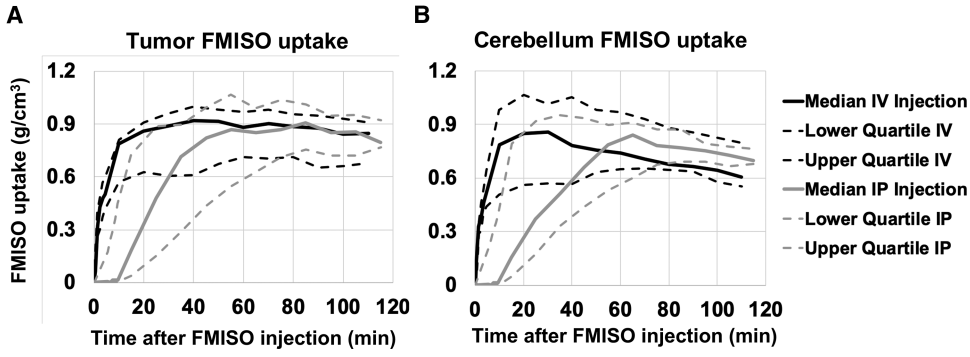

Figure 1. Median ^{18}F-fluoromisonidazo (FMISO) uptake in each dynamic positron emission tomography (PET) frame for tumors (A) and cerebellar regions (B). The gray curves show median values for rats with intraperitoneal (IP) FMISO injections (n = 8), and the black curves show median values for rats with intravenous (IV) FMISO injections (n = 10). The median tumor uptake is approximately equal for IP and IV injections after 60 minutes. The median cerebellar uptake is slightly higher for IP injections after 60 minutes.

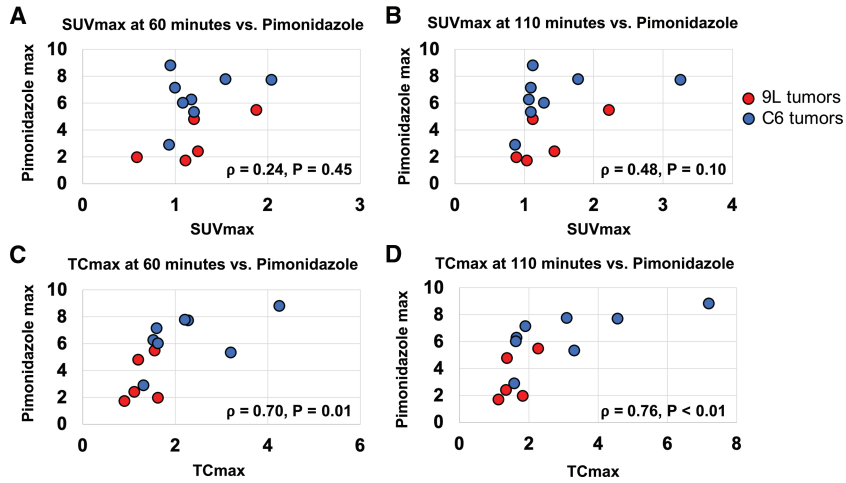

Figure 2. Scatter plots comparing FMISO PET uptake with pimonidazole fluorescence intensity in brain tumors. The top row shows correlation for the maximum PET uptake (maximum standardized uptake value) at 60 (A) and 110 (B) minutes after FMISO injection. The bottom row shows correlation for the maximum tumor-to-cerebellar ratio (TCmax) at 60 (C) and 110 (D) minutes after FMISO injection. The Spearman correlation coefficients (ρ) are shown for reference.

aforementioned references (6, 14). An analogous metric was calculated for the pimonidazole fluorescent images by extracting the maximum fluorescence intensity value from the tumor region. The SUVmax and TCmax were correlated with the maximum tumor pimonidazole intensity using Spearman correlation coefficients (Figure 2). Differences in SUVmax and TCmax between C6 and 9L tumors were assessed using Wilcoxon rank-sum tests (Table 1).

The hypoxic volume was also calculated for each tumor, as this metric has been frequently used in FMISO PET studies (4, 6, 20, 35, 38–40). PET voxels were normalized by dividing by the cerebellar uptake. The tumor volume, which included normalized PET uptake values >1.2, was considered as the tumor hypoxic volume (6, 38). The tumor hypoxic volume was found to be significantly correlated with the overall tumor volume, so the hypoxic fraction was also evaluated. The hypoxic fraction was calculated by dividing the hypoxic volume by the overall tumor volume (defined using the T2W MRI) (16). An analogous metric was derived for the pimonidazole fluorescence images by taking the fraction of fluorescence tumor voxels whose intensities were >1.5 standard deviations above the mean contralateral brain autofluorescence (termed the "pimonidazole-derived hypoxic fraction"). The FMISO hypoxic fraction was compared with the pimonidazole-derived hypoxic fraction using the Spearman correlation coefficient (Figure 3) and Lin concordance correlation coefficient to assess absolute agreement (41).

For a voxel-wise comparison, the pimonidazole fluorescence images were downsampled to the PET voxel size ($0.5 \times 0.5 \times 1$ mm). The voxel-wise correlation between PET uptake and pimonidazole intensity in tumor voxels was assessed using Spearman correlation coefficients. Correlation coefficients were calculated for each tumor and summarized for the entire population by calculating the median value (Table 2). A Wilcoxon signed-rank test assessed whether the population distribution of correlation coefficients was significantly different from zero. The slope of the FMISO uptake from 60 to 110 minutes was also calculated for each tumor voxel, as this has been used as a measure of hypoxia (7). The FMISO slope values were correlated with the pimonidazole intensity values for tumor voxels using Spearman correlation coefficients. P values <.050 were considered statistically significant.

RESULTS

Uptake curves comparing median tumor values for IP and IV FMISO injections are shown in Figure 1A. After IV injections, the median tumor uptake increased rapidly and peaked after 40 minutes. After IP injections, the median tumor uptake

Table 1. Median Values of Various ^{18}F-fluoromisonidazo Metrics for C6 and 9L Brain Tumors

Metric	Time After Injection (Minutes)	Median C6 (n = 10)	Median 9L (n = 8)	*P* Value
FMISO SUVmax	60	1.3 g/cm^3	1.2 g/cm^3	.900
	110	1.1 g/cm^3	1.1 g/cm^3	.700
FMISO TCmax	60	1.7	1.2	.002
	110	1.9	1.4	.006
FMISO hypoxic fraction	60	0.35	0.01	.001
	110	0.60	0.14	.006

Abbreviations: FMISO, ^{18}F-fluoromisonidazo; SUVmax, maximum standardized uptake value; TCmax, maximum tumor-to-cerebellar ratio.

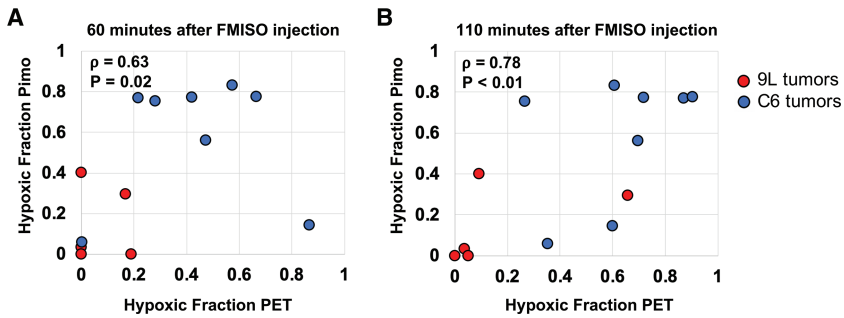

Figure 3. Scatter plots comparing the FMISO hypoxic fraction with the pimonidazole hypoxic fraction. The measurements are shown at 60 (A) and 110 (B) minutes after FMISO injection. The Spearman correlation coefficients (ρ) are shown for reference.

increased more slowly and peaked after 60 minutes. Sixty to 110 minutes after IP and IV injections, the median tumor uptake was similar for both, and the uptake decreased slightly during this time.

Uptake curves comparing median cerebellar values for IP and IV FMISO injections are shown in Figure 1B. After IV injections, the median cerebellar uptake increased rapidly and peaked after 30 minutes. After IP injections, the median cerebellar uptake increased more slowly and peaked after 60 minutes. Sixty to 110 minutes after IP injection, the median cerebellar uptake was slightly higher than for IV injections for the same time; however, both injection routes showed steady decreases in uptakes during this time. See online supplemental Figure 1 for the mean FMISO uptake curves for tumor and cerebellum.

A comparison of FMISO metrics between C6 and 9L tumors is shown in Table 1. The tumor SUVmax 60 minutes after FMISO injection was not significantly different between C6 and 9L tumors ($P = .900$); a similar result was found for the tumor SUVmax 110 minutes after FMISO injection ($P = .700$). The TCmax 60 minutes after FMISO injection was significantly greater for C6 tumors than 9L tumors ($P = .002$); similar results were found 110 minutes after FMISO injection ($P = .006$). The FMISO hypoxic fraction 60 minutes after FMISO injection was significantly greater for C6 tumors than for 9L tumors ($P = .001$); similar results were found 110 minutes after FMISO injection ($P = .006$).

In total, 13 of 18 rats had brain tissue excised for slicing, clearing, and ex vivo fluorescent imaging. Comparison of FMISO PET and pimonidazole fluorescence maximum tumor values is shown in Figure 2. FMISO SUVmax values at 60 (Figure 2A) and 110 (Figure 2B) minutes after injection were not significantly correlated with the maximum pimonidazole fluorescence intensity. Similarly, FMISO SUVmedian values were not significantly correlated with the median pimonidazole fluorescence intensity values. However, TCmax values at 60 (Figure 2C) and 110 (Figure

Table 2. Spearman Correlation Coefficients (ρ) Describing Voxel-Wise Association Between FMISO PET and Pimonidazole Fluorescence Within Tumor Regions

Tumor line	Rat	FMISO Injection Route	Tumor Volume (mm^3)	FMISO Hypoxic Volume[a] (mm^3)	FMISO Hypoxic Fraction[a]	Spearman (ρ) 60 Minutes Post Injection	Spearman (ρ) 110 Minutes Post Injection
9L	Rat 12	IV	14	0.50	0.04	+0.23	−0.10
	Rat 14	IP	11	0.54	0.05	+0.29	+0.15
	Rat 15	IP	17	0.00	0	+0.08	−0.04
	Rat 21	IV	219	144.25	0.66	+0.58	+0.63
	Rat 25	IV	119	11.00	0.09	+0.14	−0.06
C6	Rat 31	IP	24	14.50	0.60	+0.32	+0.60
	Rat 32	IV	46	39.50	0.87	+0.14	+0.40
	Rat 33	IV	17	12.00	0.72	+0.35	+0.38
	Rat 34	IV	24	8.50	0.35	−0.24	+0.27
	Rat 41	IP	63	43.75	0.69	+0.66	+0.77
	Rat 43	IV	123	74.50	0.61	+0.21	+0.37
	Rat 44	IV	90	81.25	0.90	+0.50	+0.63
	Rat 45	IP	33	8.75	0.27	+0.20	+0.23
Median			42	12.00	0.60	+0.23	+0.37

Abbreviations: IV, intravenous; IP, intraperitoneal
[a]Hypoxic volume and hypoxic fraction at 110 minutes after FMISO injection.

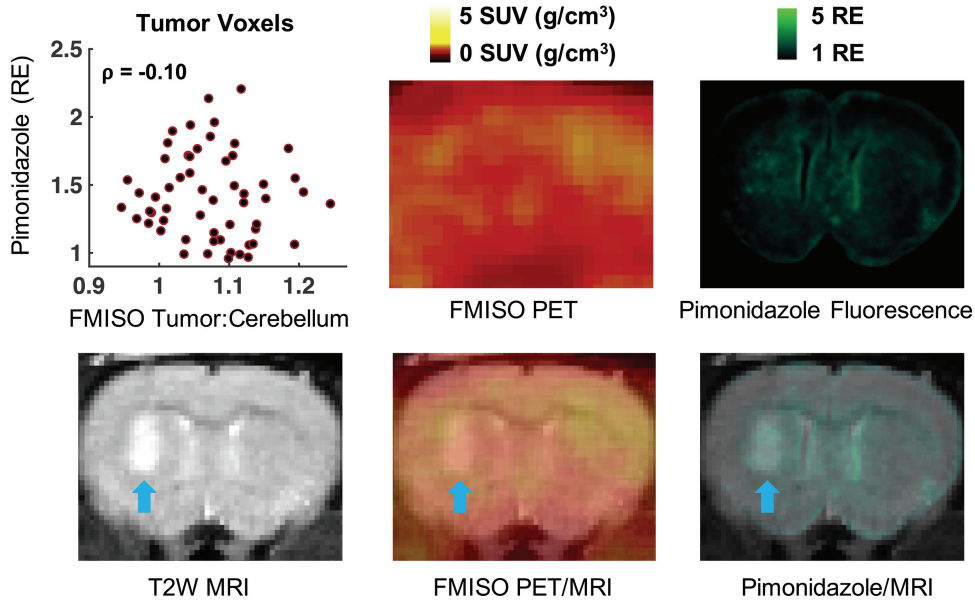

Figure 4. Coronal brain slices for rat 12 with a 9L tumor (blue arrow). The scatter plot (upper left) shows the association between FMISO PET uptake (at 110 minutes postinjection) and pimonidazole fluorescence intensity for tumor voxels. For this tumor, there was no correlation between PET uptake and pimonidazole intensity. Tumor: Cerebellum, tumor-to-cerebellum uptake ratio; RE, radiant efficiency.

2D) minutes after injection were both significantly correlated with the maximum pimonidazole intensity. The strongest correlation was for TCmax at 110 minutes, with a Spearman correlation coefficient of 0.76 ($P = .004$).

Comparison of FMISO PET and pimonidazole fluorescence tumor hypoxic fractions is shown in Figure 3. The FMISO and pimonidazole values showed a moderate Spearman correlation at 60 minutes (Figure 3A) and a stronger correlation at 110 minutes (Figure 3B) after FMISO injection. The Lin concordance correlation coefficients between FMISO- and pimonidazole-measured hypoxic fractions were 0.42 (95%CI, 0.09–0.76) and 0.69 (95%CI, 0.25–0.89) at 60 and 110 minutes after FMISO injection, respectively.

Table 2 shows voxel-wise correlations between FMISO PET uptake and pimonidazole fluorescence intensity in tumor regions. The median voxel-wise Spearman correlation coefficient across all tumors was 0.24 ($P = .004$) 60 minutes after FMISO injection and 0.37 ($P = .003$) 110 minutes after FMISO injection. However, there was variability across tumors, with some tumors showing no correlation and some tumors showing a strong positive correlation between FMISO and pimonidazole (see the range of values in Table 2). The voxel-wise correlation between FMISO and pimonidazole for a given tumor was significantly dependent on the tumor's hypoxic fraction ($\rho = 0.58$, $P = .040$) 60 minutes after FMISO injection. The voxel-wise correlation between FMISO and pimonidazole for a given tumor was significantly dependent on the TCmax ($\rho = 0.81$, $P = .0009$) and the tumor hypoxic fraction ($\rho = 0.85$, $P = .0003$) 110 minutes after FMISO injection. The voxel-wise correlation between FMISO and pimonidazole for a given tumor was *not significantly* dependent on the FMISO injection route (IP vs IV), tumor volume, or tumor SUVmax. The FMISO uptake slope from 60 to 110 minutes also showed a positive correlation with the pimonidazole intensity values, with the median voxel-wise Spearman correlation coefficient across all tumors being 0.31 ($P = .02$).

Figure 4 shows the registered images for a 9L tumor that showed *no voxel-wise correlation* between FMISO uptake and pimonidazole intensity. Figure 5 shows the registered images for a C6 tumor that showed a *moderate* voxel-wise correlation between FMISO uptake and pimonidazole intensity. Figure 6 shows the registered images for a 9L tumor that showed a *strong* voxel-wise correlation between FMISO uptake and pimonidazole intensity.

DISCUSSION

This study provides the first cross-validation of in vivo image-derived hypoxia metrics with an ex vivo hypoxia reference standard across whole tumor volumes. This analysis further establishes the reliability of hypoxia metrics derived from FMISO PET images and sheds insight on their clinical utility. Although numerous reports have verified that FMISO provides a clinically useful measure of hypoxia, no study to our knowledge has spatially correlated FMISO uptake with an ex vivo reference standard for hypoxia across whole tumor volumes. Previous attempts to spatially validate image-derived measures of hypoxia have relied on autoradiography that provides cross-validation between radiotracers and pimonidazole antibodies at the microregional level (18, 19, 31). However, although autoradiography provides excellent cross-validation at a microregional level, it has a number of limitations:

(1) It makes no direct comparison between in vivo images and ex vivo reference standards.

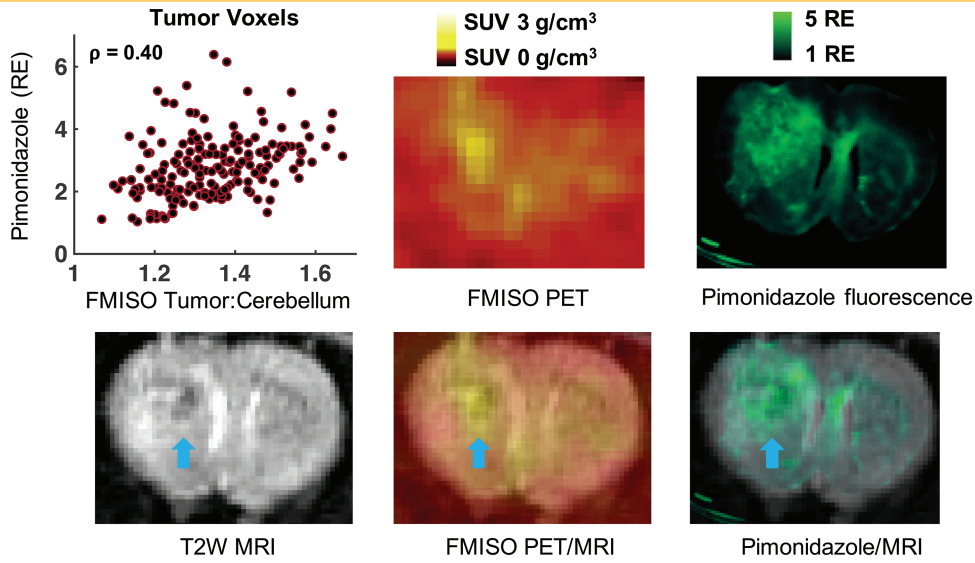

Figure 5. Coronal brain slices of rat 32 with a C6 tumor (blue arrow). The scatter plot shows the association between FMISO PET uptake (at 110 minutes postinjection) and pimonidazole fluorescence intensity for tumor voxels. For this tumor, there was moderate positive correlation between PET uptake and pimonidazole intensity. Tumor: Cerebellum, tumor-to-cerebellum uptake ratio; RE, radiant efficiency.

(2) It provides no way of evaluating imaging techniques that do not use radiotracers (eg, MRI).
(3) It is performed on thin histologic sections that can be challenging to acquire across whole organs or tumors, even in preclinical studies.

To overcome these limitations, a method was recently developed to coregister in vivo medical images with ex vivo optical reporter images of cleared tissue (32). Here, that method was used to compare FMISO PET metrics of hypoxia with analogous pimonidazole fluorescence metrics across the whole tumor.

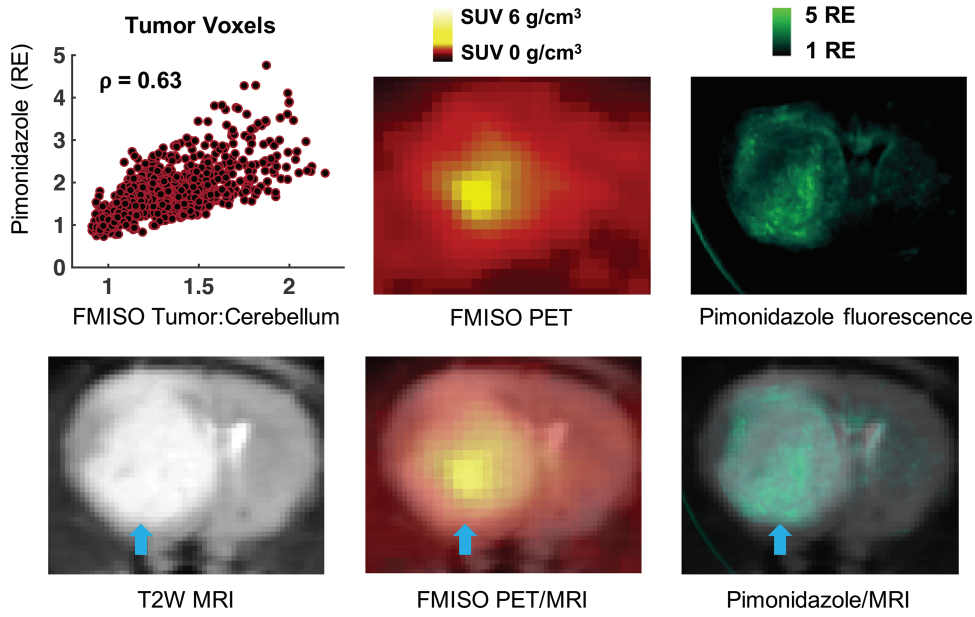

Figure 6. Coronal brain slices of rat 21 with a 9L tumor (blue arrow). The scatter plot shows the association between FMISO PET uptake (at 110 minutes postinjection) and pimonidazole fluorescence intensity for tumor voxels. For this tumor, there was a strong positive correlation between PET uptake and pimonidazole intensity. Tumor: Cerebellum, tumor to cerebellum uptake ratio; RE, radiant efficiency.

Across 13 rat brain tumors, the voxel-wise analysis revealed a modest positive correlation between FMISO PET uptake and pimonidazole fluorescence intensity. However, the results varied greatly across tumors, with some tumors showing a strong positive correlation and other tumors showing no correlation. Using autoradiography, a previous study by Troost et al. (18) found a weak-to-moderate pixel-by-pixel correlation between FMISO uptake and pimonidazole immunohistochemistry in subcutaneous brain tumors. Troost et al. (18) suggested that using only 60 minutes of FMISO uptake time may have limited the correlation between FMISO and pimonidazole staining found in their study. This is supported by the results of this study, with only weak-to-moderate correlation between FMISO PET and pimonidazole fluorescence found after 60 minutes of FMISO uptake. Furthermore, after 110 minutes of FMISO uptake, a stronger correlation between FMISO uptake and pimonidazole fluorescence was found. This trend held true for the voxel-level measures and for the tumor summarized metrics (eg, tumor hypoxic fraction). This indicates that static FMISO PET frames acquired at later time points post injection (after 60 minutes) provide a more accurate measure of the spatial distribution of hypoxia within tumors, which agrees with results from previous studies (14). The reason for more accurate hypoxia measures at later time points is likely due to increased washout of FMISO from the blood compartment at later time points, providing increased specificity to bound FMISO (ie, hypoxic regions) (6). FMISO PET imaging at time points later than 110 minutes after injection may further improve correlations with the pimonidazole reference standard (14, 42). However, it was not possible to test within this study because of tracer decay and timing limitations that arose from scanning multiple subjects within a single day.

The majority of previous brain cancer studies using FMISO PET have attempted to improve quantification of hypoxia by normalizing the FMISO tumor activity by the blood activity (4–6, 13, 14, 17, 20, 38–40, 42–44). Traditionally, the FMISO blood activity has been measured by blood sampling; however, recently, it was shown that FMISO cerebellar activity can be used as a surrogate for FMISO blood 3activity at later time points post injection (6). We found that normalization of the tumor FMISO activity by the cerebellar activity greatly improved the correlation between FMISO PET metrics and pimonidazole fluorescence imaging metrics. Most notably, there was a strong positive correlation between the FMISO TCmax and the maximum pimonidazole fluorescence intensity. The more conventional metric, the tumor SUVmax, was not significantly correlated with the maximum pimonidazole fluorescence intensity. These results support the notion that the cerebellum can be used as a surrogate for FMISO blood activity, and its use can significantly improve estimates of tumor hypoxia. One uncertainty that remains is because of the relatively low spatial resolution of the PET images that leads to partial volume effects and hindered quantification of small hypoxic regions (45). However, the strong correlation between the TCmax and pimonidazole max suggests that despite these effects, FMISO PET images can still provide reliable assessment of the most hypoxic tumor region.

Another metric that has been widely used in FMISO PET research is the tumor hypoxic volume (4, 6, 20, 35, 38–40). The FMISO hypoxic volume is calculated as the volume of tumor that is above a certain PET uptake threshold (after normalization by the FMISO blood or cerebellar activity). In this study, the FMISO tumor hypoxic volume was significantly correlated with the overall tumor volume (defined using the T2W MRI), suggesting that it may not provide a reliable assessment of the tumor's hypoxic status. Therefore, the analysis focused on the tumor hypoxic fraction, as it was less dependent on the overall tumor volume (16). A strong concordance between the FMISO tumor hypoxic fraction and the pimonidazole-derived hypoxic fraction was found, indicating good absolute agreement between the 2 measurements. This supports utilization of the FMISO hypoxic fraction as a marker of tumor hypoxia and for comparing the degree of hypoxia across tumors.

Interestingly, the greater a tumor's hypoxic fraction the stronger the voxel-level correlation between FMISO and pimonidazole images. This suggests that FMISO measurements in individual tumor voxels are more accurate in tumors showing a greater hypoxic fraction. These tumors are likely the best candidates for image-guided radiotherapy based on boosting dose to radio-resistant hypoxic tumor regions (11, 12). It is not surprising that the voxel-level correlation between FMISO and pimonidazole images is worse in tumors with less hypoxia. Misonidazole has been shown to be sensitive to hypoxia only when oxygen tension values are $<$3–10 mm Hg, suggesting that tumors with low levels of hypoxia (ie, tumors with oxygen tension $>$3–10 mm Hg) will not be reliably assessed with FMISO or pimonidazole imaging techniques (16, 46).

In preclinical studies, IP radiotracer injections offer some advantages over IV injections. IP injections can be technically easier to implement, as they do not require insertion of a catheter or needle into a vein for tracer administration. IP injections also enable a greater volume of tracer to be injected that can be particularly advantageous if radiotracer concentrations are low (eg, at the end of the day when scanning multiple subjects with a single batch of radiotracer). This study showed that after 60 minutes, the median tumor FMISO uptake was similar for IP and IV injections. The results also showed that the correlations between the ex vivo pimonidazole reference and FMISO PET images were not dependent on the injection route (IP vs IV), suggesting that the IP injection could be a valid alternative to IV injections when imaging rat brain tumors.

A limitation of this work is that the tissue clearing procedures could be washing out pimonidazole adducts and, therefore, diminish the correlation between FMISO and pimonidazole. However, the greater degree of pimonidazole staining seen on the C6 tumors relative to 9L tumors, which agrees with previous literature, provides evidence that the pimonidazole adducts are not being washed out. The strong correlation between the pimonidazole and FMISO PET provides further evidence that the pimonidazole adducts are not being washed out. An additional limitation of this work is that we used animal models of glioma (9L and C6 tumors), which may provide slightly different relationships between FMISO PET and pimonidazole fluorescence than human glioma cells. However, no previous study had evaluated the correlation between FMISO uptake and pimonidazole staining in C6 and 9L tumors, despite the widespread utilization of these cell lines in preclinical studies (7, 17, 33, 34). Therefore, these results provide a valuable reference for previous and future

studies aiming to use FMISO PET with these glioma cell lines. Consistent with the previous studies, this study showed that, in general, C6 tumors showed greater hypoxia (based on both FMISO PET and pimonidazole measurements) than 9L tumors (7). However, there were exceptions, with some 9L tumors showing elevated FMISO PET and pimonidazole fluorescence measurements (eg, Figure 6).

In conclusion, in vivo FMISO PET images were registered to ex vivo fluorescence pimonidazole images of optically cleared brain tissue to evaluate the regional correlation between the 2 imaging techniques. These results can serve as a platform for cross-validating other promising hypoxia imaging methods such as fluorine-18-labeled [2-(2-nitro-1[H]-imidazol-1-yl)- N-(2,2,3,3,3-pentafluoropropyl)-acetamide] (EF5) PET (10). EF5 is more lipophilic than FMISO, which offers potential advantages for PET imaging, as it can more readily enter tissues. Thus, EF5 could show greater correlations with pimonidazole than with FMISO. The results here showed a moderate voxel-wise correlation between FMISO PET uptake and pimonidazole fluorescence intensity; however, the results varied greatly across individual tumors. A strong correlation between the maximum FMISO TCmax and the maximum pimonidazole intensity was identified. Similarly, a strong correlation between the FMISO-derived hypoxic fraction and the pimonidazole-derived hypoxic fraction was found. These results can be used to better inform clinical use of FMISO PET and, in particular, identify the most reliable imaging metrics of hypoxia.

Supplemental Materials

Supplemental Figure 1: https://doi.org/10.18383/j.tom.2020.00046.sup.01

ACKNOWLEDGMENTS

This work was sponsored by Barrow Neurological Foundation, the Dignity Health and Arizona State University Collaborative Strategic Initiative and the Arizona Biomedical Research Centre (ADHS18-198850). We wish to thank the Banner Alzheimer's Institute's Cyclotron and Radiochemistry Laboratory for providing the PET tracer for these studies.

Conflict of Interest: None reported.

Disclosures: No disclosures to report.

REFERENCES

1. Merighi S, Benini A, Mirandola P, Gessi S, Varani K, Leung E, Maclennan S, Baraldi PG, Borea PA. Hypoxia inhibits paclitaxel-induced apoptosis through adenosine-mediated phosphorylation of bad in glioblastoma cells. Mol Pharmacol. 2007;72:162–172.
2. Chen Z, Htay A, Santos WD, Gillies GT, Fillmore HL, Sholley MM, Broaddus WC. In vitro angiogenesis by human umbilical vein endothelial cells (HUVEC) induced by three-dimensional co-culture with glioblastoma cells. J Neurooncol. 2009;92:121–128.
3. Mendichovszky I, Jackson A. Imaging hypoxia in gliomas. Br J Radiol. 2011;84: S145–S158.
4. Spence AM, Muzi M, Swanson KR, O'Sullivan F, Rockhill JK, Rajendran JG, Adamsen TCH, Link JM, Swanson PE, Yagle KJ, Rostomily RC, Silbergeld DL, Krohn KA. Regional hypoxia in glioblastoma multiforme quantified with [18F]fluoromisonidazole positron emission tomography before radiotherapy: correlation with time to progression and survival. Clin Cancer Res. 2008;14:2623–2630.
5. Gerstner ER, Zhang Z, Fink JR, Muzi M, Hanna L, Greco E, Prah M, Schmainda KM, Mintz A, Kostakoglu L, Eikman EA, Ellingson BM, Ratai E-M, Sorensen AG, Barboriak DP, Mankoff DA. ACRIN 6684: assessment of tumor hypoxia in newly diagnosed glioblastoma using 18F-FMISO PET and MRI. Clin Cancer Res. 2016;22:5079–5086.
6. Muzi M, Peterson LM, O'Sullivan JN, Fink JR, Rajendran JG, McLaughlin LJ, Muzi JP, Mankoff DA, Krohn KA. 18F-Fluoromisonidazole quantification of hypoxia in human cancer patients using image-derived blood surrogate tissue reference regions. J Nucl Med. 2015;56:1223–1228.
7. Stokes AM, Hart CP, Quarles CC. Hypoxia imaging with PET correlates with antitumor activity of the hypoxia-activated prodrug evofosfamide (TH-302) in rodent glioma models. Tomography. 2016;2:229–237.
8. Linnik IV, Scott MLJ, Holliday KF, Woodhouse N, Waterton JC, O'Connor JPB, Barjat H, Liess C, Ulloa J, Young H, Dive C, Hodgkinson CL, Ward T, Roberts D, Mills SJ, Thompson G, Buonaccorsi GA, Cheung S, Jackson A, Naish JH, Parker GJM. Noninvasive tumor hypoxia measurement using magnetic resonance imaging in murine U87 glioma xenografts and in patients with glioblastoma. Magn Reson Med. 2014;71:1854–1862.
9. Gulaka PK, Rojas-Quijano F, Kovacs Z, Mason RP, Sherry AD, Kodibagkar VD. GdDO3NI, a nitroimidazole-based T1 MRI contrast agent for imaging tumor hypoxia in vivo. J Biol Inorg Chem. 2014;19:271–279.
10. Ziemer L, Evans S, Kachur A, Shuman A, Cardi C, Jenkins W, Karp J, Alavi A, Dolbier W, Koch C. Noninvasive imaging of tumor hypoxia in rats using the 2-nitroimidazole 18F-EF5. Eur J Nucl Med Mol Imaging. 2003;30:259–266.
11. Gérard M, Corroyer-Dulmont A, Lesueur P, Collet S, Chérel M, Bourgeois M, Thariat J, Valable S. Hypoxia imaging and adaptive radiotherapy: a state-of-the-art approach in the management of glioma. Front Med (Lausanne). 2019;6:117.
12. Chang JH, Wada M, Anderson NJ, Lim Joon D, Lee ST, Gong SJ, Gunawardana DH, Sachinidis J, O'Keefe G, Gan HK, Khoo V, Scott AM. Hypoxia-targeted radiotherapy dose painting for head and neck cancer using (18)F-FMISO PET: a biological modeling study. Acta Oncol. 2013;52:1723–1729.
13. Valk PE, Mathis CA, Prados MD, Gilbert JC, Budinger TF. Hypoxia in human gliomas: demonstration by PET with fluorine-18-fluoromisonidazole. J Nucl Med. 1992;33:2133–2137.
14. Bruehlmeier M, Roelcke U, Schubiger PA, Ametamey SM. Assessment of hypoxia and perfusion in human brain tumors using PET with 18F-fluoromisonidazole and 15O-H2O. J Nucl Med. 2004;45:1851–1859.
15. Rasey JS, Grunbaum Z, Magee S, Nelson NJ, Olive PL, Durand RE, Krohn KA. Characterization of radiolabeled fluoromisonidazole as a probe for hypoxic cells. Radiat Res. 1987;111:292–304.
16. Rasey JS, Casciari JJ, Hofstrand PD, Muzi M, Graham MM, Chin LK. Determining hypoxic fraction in a rat glioma by uptake of radiolabeled fluoromisonidazole. Radiat Res. 2000;153:84–92.
17. Tochon-Danguy HJ, Sachinidis JI, Chan F, Gordon Chan J, Hall C, Cher L, Stylli S, Hill J, Kaye A, Scott AM. Imaging and quantitation of the hypoxic cell fraction of viable tumor in an animal model of intracerebral high grade glioma using [18F]fluoromisonidazole (FMISO). Nucl Med Biol. 2002;29:191–197.
18. Troost EGC, Laverman P, Kaanders JHAM, Philippens M, Lok J, Oyen WJG, van der Kogel AJ, Boerman OC, Bussink J. Imaging hypoxia after oxygenation-modification: comparing [18F]FMISO autoradiography with pimonidazole immunohistochemistry in human xenograft tumors. Radiother Oncol. 2006;80:157–164.
19. Troost EGC, Laverman P, Philippens MEP, Lok J, van der Kogel AJ, Oyen WJG, Boerman OC, Kaanders JHAM, Bussink J. Correlation of [18F]FMISO autoradiography and pimonidazole [corrected] immunohistochemistry in human head and neck carcinoma xenografts. Eur J Nucl Med Mol Imaging. 2008;35:1803–1811.
20. Swanson KR, Chakraborty G, Wang CH, Rockne R, Harpold HLP, Muzi M, Adamsen TCH, Krohn KA, Spence AM. Complementary but distinct roles for MRI and 18F-fluoromisonidazole PET in the assessment of human glioblastomas. J Nucl Med. 2008;50:36–44.
21. Krohn KA, Link JM, Mason RP. Molecular imaging of hypoxia. J Nucl Med. 2008;49:129S–148S.
22. Martin GV, Cerqueira MD, Caldwell JH, Rasey JS, Embree L, Krohn KA. Fluoromisonidazole. A metabolic marker of myocyte hypoxia. Circ Res. 1990;67:240–244.
23. Bell C, Dowson N, Fay M, Thomas P, Puttick S, Gal Y, Rose S. Hypoxia imaging in gliomas with 18F-fluoromisonidazole PET: toward clinical translation. Semin Nucl Med. 2015;45:136–150.
24. Nehmeh SA, Lee NY, Schröder H, Squire O, Zanzonico PB, Erdi YE, Greco C, Mageras G, Pham HS, Larson SM, Ling CC, Humm JL. Reproducibility of intratumor

distribution of (18)F-fluoromisonidazole in head and neck cancer. Int J Radiat Oncol Biol Phys. 2008;70:235–242.
25. Masaki Y, Shimizu Y, Yoshioka T, Tanaka Y, Nishijima K-I, Zhao S, Higashino K, Sakamoto S, Numata Y, Yamaguchi Y, Tamaki N, Kuge Y. The accumulation mechanism of the hypoxia imaging probe "FMISO" by imaging mass spectrometry: possible involvement of low-molecular metabolites. Sci Rep. 2015;5:16802.
26. Arteel GE, Thurman RG, Raleigh JA. Reductive metabolism of the hypoxia marker pimonidazole is regulated by oxygen tension independent of the pyridine nucleotide redox state. Eur J Biochem. 1998;253:743–750.
27. Lokmic Z, Musyoka J, Hewitson TD, Darby IA. Hypoxia and hypoxia signaling in tissue repair and fibrosis. Int Rev Cell Mol Biol. 2012;296:139–185.
28. Raleigh JA, Chou SC, Arteel GE, Horsman MR. Comparisons among pimonidazole binding, oxygen electrode measurements, and radiation response in C3H mouse tumors. Radiat Res. 1999;151:580–589.
29. Pogue BW, Paulsen KD, O'Hara JA, Wilmot CM, Swartz HM. Estimation of oxygen distribution in RIF-1 tumors by diffusion model-based interpretation of pimonidazole hypoxia and eppendorf measurements. Radiat Res. 2001;155:15–25.
30. Corroyer-Dulmont A, Pérès EA, Petit E, Durand L, Marteau L, Toutain J, Divoux D, Roussel S, MacKenzie ET, Barré L, Bernaudin M, Valable S. Noninvasive assessment of hypoxia with 3-[18F]-fluoro-1-(2-nitro-1-imidazolyl)-2-propanol ([18F]-FMISO): a PET study in two experimental models of human glioma. Biol Chem. 2013;394:529–539.
31. Hatano T, Zhao S, Zhao YAN, Nishijima K-I, Kuno N, Hanzawa H, Sakamoto T, Tamaki N, Kuge YUJI. Biological characteristics of intratumoral [F-18]-fluoromisonidazole distribution in a rodent model of glioma. Int J Oncol. 2013;42:823–830.
32. Scarpelli ML, Healey DR, Mehta S, Kodibagkar VD, Quarles CC. A practical method for multimodal registration and assessment of whole-brain disease burden using PET, MRI, and optical imaging. Sci Rep. 2020;10:17324.
33. Benda P, Lightbody J, Sato G, Levine L, Sweet W. Differentiated rat glial cell strain in tissue culture. Science. 1968;161:370–371.
34. Benda P, Someda K, Messer J, Sweet WH. Morphological and immunochemical studies of rat glial tumors and clonal strains propagated in culture. J Neurosurg. 1971;34:310–323.
35. Valable S, Petit E, Roussel S, Marteau L, Toutain J, Divoux D, Sobrio F, Delamare J, Barré L, Bernaudin M. Complementary information from magnetic resonance imaging and (18)F-fluoromisonidazole positron emission tomography in the assessment of the response to an antiangiogenic treatment in a rat brain tumor model. Nucl Med Biol. 2011;38:781–793.
36. Scarpelli M, Eickhoff J, Cuna E, Perlman S, Jeraj R. Optimal transformations leading to normal distributions of positron emission tomography standardized uptake values. Phys Med Biol. 2018;63:035021.
37. Thie JA, Hubner KF, Smith GT. The diagnostic utility of the lognormal behavior of PET standardized uptake values in tumors. J Nucl Med. 2000;41:1664–1672.
38. Rajendran JG, Mankoff DA, O'Sullivan F, Peterson LM, Schwartz DL, Conrad EU, Spence AM, Muzi M, Farwell DG, Krohn KA. Hypoxia and glucose metabolism in malignant tumors: evaluation by [18F]fluoromisonidazole and [18F]fluorodeoxyglucose positron emission tomography imaging. Clin Cancer Res. 2004;10:2245–2252.
39. Bekaert L, Valable S, Lechapt-Zalcman E, Ponte K, Collet S, Constans J-M, Levallet G, Bordji K, Petit E, Branger P, Emery E, Manrique A, Barré L, Bernaudin M, Guillamo J-S. 18F]-FMISO PET study of hypoxia in gliomas before surgery: correlation with molecular markers of hypoxia and angiogenesis. Eur J Nucl Med Mol Imaging. 2017;44:1383–1392.
40. Kawai N, Lin W, Cao W-D, Ogawa D, Miyake K, Haba R, Maeda Y, Yamamoto Y, Nishiyama Y, Tamiya T. Correlation between ^{18}F-fluoromisonidazole PET and expression of HIF-1α and VEGF in newly diagnosed and recurrent malignant gliomas. Eur J Nucl Med Mol Imaging. 2014;41:1870–1878.
41. Lin LI. A concordance correlation coefficient to evaluate reproducibility. Biometrics. 1989;45:255–268.
42. Hirata K, Terasaka S, Shiga T, Hattori N, Magota K, Kobayashi H, Yamaguchi S, Houkin K, Tanaka S, Kuge Y, Tamaki N. ^{18}F-Fluoromisonidazole positron emission tomography may differentiate glioblastoma multiforme from less malignant gliomas. Eur J Nucl Med Mol Imaging. 2012;39:760–770.
43. Tong X, Srivatsan A, Jacobson O, Wang Y, Wang Z, Yang X, Niu G, Kiesewetter DO, Zheng H, Chen X. Monitoring tumor hypoxia using (18)F-FMISO PET and pharmacokinetics modeling after photodynamic therapy. Sci Rep. 2016;6:31551.
44. Yamamoto Y, Maeda Y, Kawai N, Kudomi N, Aga F, Ono Y, Nishiyama Y. Hypoxia assessed by 18F-fluoromisonidazole positron emission tomography in newly diagnosed gliomas. Nucl Med Commun. 2012;33:621–625.
45. Cherry S, Sorenson J, Phelps M. Physics in Nuclear Medicine. Fourth ed. Philadelphia, PA: Elsevier; 2012.
46. Gross MW, Karbach U, Groebe K, Franko AJ, Mueller-Klieser W. Calibration of misonidazole labeling by simultaneous measurement of oxygen tension and labeling density in multicellular spheroids. Int J Cancer. 1995;61:567–573.